
PET with ^{18}F -FDG–Labeled T Lymphocytes for Diagnosis of Acute Rat Renal Allograft Rejection

Alexander Grabner*¹, Dominik Kentrup*¹, Bayram Edemir¹, Yasemin Sirin¹, Hermann Pavenstädt¹, Eberhard Schlatter¹, Otmar Schober², Michael Schäfers³, Uta Schnöckel², and Stefan Reuter¹

¹Department of Internal Medicine D, Experimental Nephrology, University of Münster, Münster, Germany; ²Department of Nuclear Medicine, University of Münster, Münster, Germany; and ³European Institute for Molecular Imaging, University of Münster, Münster, Germany

We proposed small-animal PET with ^{18}F -FDG–labeled T lymphocytes as a new method for image-based diagnosis of acute allogeneic renal transplant rejection (AR) established in a rat model.

Methods: One and 2 h after tail vein injection of 30×10^6 ex vivo ^{18}F -FDG–labeled human T cells into male 10-wk-old uninephrectomized, allogeneically transplanted rats (aTX; Lewis–brown Norway [LBN] to Lewis), whole-body radioactivity distribution was assessed in vivo by small-animal PET (postoperative day 4), and percentage injected dose (%ID) as a parameter of T-cell infiltration was assessed and compared between graft and native kidney. In vivo results were confirmed by autoradiography and staining of human CD3 after postmortem dissection. Syngeneically transplanted rats (sTX) (LBN to LBN), rats with ischemia–reperfusion injury (IRI) (45-min warm ischemia), and rats subjected to acute cyclosporine A (CSA) toxicity (50 mg/kg for 2 d intraperitoneally) served as controls. **Results:** The accumulation of labeled cells was significantly elevated in allografts with AR (1.07 ± 0.28 %ID), compared with native control kidneys (0.49 ± 0.18 %ID) ($P < 0.0001$). No differences were found among native controls, sTX, CSA toxicity, and kidneys with IRI. In vivo uptake of ^{18}F -FDG cells measured in the PET scanner correlated with results obtained by autoradiography, histologic evaluation, and polymerase chain reaction. **Conclusion:** We proposed graft PET imaging using ^{18}F -FDG–labeled T cells as a new option to detect rat renal AR with a low dose of ^{18}F -FDG in a noninvasive, fast, and specific manner in rats.

Key Words: renal transplantation; acute rejection; radiolabeled T lymphocytes; ^{18}F -FDG; PET

J Nucl Med 2013; 54:1147–1153

DOI: 10.2967/jnumed.112.109231

At present, diagnosis of acute transplant rejection (AR) in humans relies on graft biopsy on renal allograft dysfunction (1,2). However, more than 50% of the rejection episodes are subclinical, without acute impairment of renal function and, interestingly, with a histologic severity score that was found to be comparable

to that of patients with a decrease in glomerular filtration rate during AR (3). Therefore, one may undergo protocol biopsies at a defined time course after transplantation, irrespective of the status of graft function, to diagnose AR (2). Biopsy is an invasive procedure that is cumbersome to the patient, carries the risk of graft injury, and is not feasible in recipients taking anticoagulant medication (4,5). In addition, the sampling site is small and AR may be missed (i.e., when rejection is focal or patchy) (6). Thus, in diagnostics, entirely image-based methods visualizing the whole organ would be superior. Nuclear imaging approaches including SPECT and PET have the advantages of high intrinsic sensitivity, excellent tissue penetration, and a wide range of clinically available molecular imaging probes (7). Recently, we have established ^{18}F -FDG PET as an entirely image-based method to assess and to monitor acute renal rejection (8,9). However, potential drawbacks in applying ^{18}F -FDG PET to the clinical setting should be noted. First, urinary excretion of the tracer necessitates late acquisitions to reduce the amount of ^{18}F -FDG in the urine. Further, the renal pelvis should be carefully excluded from the measurements. Second, ^{18}F -FDG uptake is not disease-specific. Thus, a more specific method is desirable.

AR results from interactions between the recipient's immune system and the foreign antigens serving as a target. T lymphocytes (CD4^+ and CD8^+) are central and specific to the AR process, whereas B cells and the congenital immune system (e.g., complement, monocytes and macrophages, neutrophils, and dendritic cells) participate (10,11). After recognition of donor-derived antigens, T cells migrate into the transplant and infiltrate the interstitial space (12). Because recruitment and activation of inflammatory cells, in particular lymphocytes, play decisive roles in AR, efforts have already been made to image infiltration by means of radiolabeled leukocytes (7). Because infiltration of leukocytes, especially T lymphocytes in allografts, appears before physiologic or mechanical manifestations of organ dysfunction is apparent, nuclear imaging using lymphocytes might be a promising tool for sensitive and early detection of rejection. However, PET with ^{18}F -FDG–labeled T lymphocytes for diagnosis of AR has never been tested before. Thus, we applied PET with ^{18}F -FDG–labeled human T lymphocytes in an established rat renal transplant model (9). ^{18}F -FDG uptake of the renal parenchyma was assessed on postoperative day 4 (POD4) in uninephrectomized, allogeneically kidney-transplanted animals (aTX) with, and additionally in native controls and syngeneically transplanted (sTX) animals without, rejection or impairment of renal function. Because acute cyclosporine A (CSA) nephrotoxicity and acute tubular necrosis (ATN) caused by ischemia–reperfusion injury (IRI) are important

Received May 22, 2012; revision accepted Nov. 12, 2012.

For correspondence or reprints contact: Stefan Reuter, Medizinische Klinik und Poliklinik D, Albert-Schweitzer-Campus 1, D 48149 Münster, Germany. E-mail: sreuter@uni-muenster.de

*Contributed equally to this work.

†Contributed equally to this work.

Published online May 13, 2013.

COPYRIGHT © 2013 by the Society of Nuclear Medicine and Molecular Imaging, Inc.

differential diagnoses of AR, we have included these 2 additional groups into the study.

MATERIALS AND METHODS

Animal Models

Surgical and imaging experiments were approved by a government committee on animal welfare and performed in accordance with national animal protection guidelines. Male Lewis–Brown Norway (LBN) and Lewis (LEW) rats (200–270 g of body weight; Charles River) with free access to standard rat chow (Altromin) and tap water were used. Surgeries were performed under anesthesia with ketamine (100 mg/kg of body weight intraperitoneally) and xylazine (5 mg/kg of body weight intraperitoneally) (Xylazin and Ketamin; CEVA Tiergesundheits). Further doses of ketamine were injected as needed.

Transplantation was simultaneously performed by 2 investigators as published before (9,13,14). In short, the left kidney including ureter, renal artery, a piece of aorta, and renal vein were transferred into the recipient. Kidneys from age- and weight-matched LBN rats were transplanted into LEW rats (aTX). Transplantations were performed immediately after left nephrectomy of the recipient. Although the total operation time of the recipient did not exceed 90 min, the ischemia time of the graft was always shorter than 40 min. Grafts were studied on POD4 after transplantation. The chosen aTX model leads to histologic and functional changes typical for AR (9,13,14). As in the model cited by those studies without immunosuppression, graft necrosis starts only a few days beyond POD4; thus, we decided to investigate kidneys on POD4. Syngeneically transplanted rats (LBN to LBN, sTX) without AR served as controls. Because ATN and acute CSA toxicity are common differential diagnoses of AR, these groups have been also included. ATN (induced by IRI) and acute CSA toxicity were induced as published before (9,15). For IRI, the left renal artery was dissected as in transplant groups and ligated for 45 min using a microvascular clamp. After clamp release, the return of original surface color of the kidneys was confirmed visually. For acute CSA-induced nephrotoxicity, rats received 50 mg of CSA per kilogram (Sandimmun; Novartis) intraperitoneally for 2 d.

T-Cell Isolation and Labeling

^{18}F -FDG was produced in a clinical routine setup on-site using an RDS 111 cyclotron (CTI). T lymphocytes were isolated from human buffycoats (containing mainly white and red blood cells and platelets) (DRK Münster) by negative antibody selection using the RosetteSep method according to the manufacturer's protocol (Stemcell). After cell numbers were counted in a Neubauer chamber, cells were adjusted to the desired amount, incubated with 80–120 MBq of ^{18}F -FDG for 30 min, washed twice with phosphate buffer, and finally resuspended in 300 μL of physiologic saline for further experiments.

For analysis of labeling efficiency, 5×10^6 T cells were incubated for 30 min either with 7 MBq of ^{18}F -FDG in physiologic saline or with K^+ -enriched solution (Sterofundin; Braun) in the presence or absence of insulin (10 IU). After centrifugation, radioactivity in the supernatant and pelleted cells was measured by γ -counting, and labeling efficiency was calculated as the ratio between radioactivity in cells and overall radioactivity.

For analysis of labeling stability, 5×10^6 T cells labeled with 7 MBq of ^{18}F -FDG as described before were incubated in blood plasma for 10, 30, 60, and 120 min. After incubation, samples were centrifuged, and radioactivity in the supernatant and pelleted cells was measured by γ -counting. Labeling stability was calculated as percentage share of radioactivity in cells per supernatant on the basis of total radioactivity.

Image Acquisition: PET

Image acquisition of nonfasting subjects was performed as described before (8,9). In short, T-cell infiltration was calculated from a whole-body acquisition of 20 min at 1 and 2 h after injection of 30×10^6 ex vivo ^{18}F -FDG-labeled human T cells (1–2 MBq of ^{18}F -FDG) in 300 μL of 0.9% NaCl solution into a tail vein. Thereafter, the catheter was purged with an additional 700 μL of 0.9% NaCl solution. Rats remained in a restrainer under anesthesia until the start of the scan. During acquisition, rats were further anesthetized with oxygen–isoflurane inhalation (2% isoflurane, 0.7 l/min oxygen), and body temperature was maintained at physiologic values by a heating pad. Scans were obtained using a PET camera with a high-resolution multi-wire chamber (quadHIDAC; Oxford Positron Systems Ltd.) (16).

PET Image Analysis and Quantitative Evaluation

A renal parenchyma volume of interest was manually traced around the kidneys on reconstructed coronal images. Mean ^{18}F -FDG T-cell activity of the renal parenchyma was calculated by the ratio of total counts and volume.

Autoradiography

To validate the data obtained by PET, animals were sacrificed and kidneys were excised immediately after PET scanning. High-resolution autoradiography (μ -imager; Biospace Measures) was performed as published before (9). In short, kidneys were snap-frozen and sliced into 10- μm -thick cryosections, and the radioactivity was measured in a mid-coronary renal slice for 3 h.

Histology

Portions of kidneys were snap-frozen and fixed in 4% formaldehyde in phosphate-buffered saline. Histologic changes (glomerulitis, tubulitis, endothelialitis, and infiltration) were examined by light microscopy in paraffin-embedded tissue with periodic acid-Schiff and hematoxylin and eosin staining. For the evaluation, only the cortex was chosen because the extent of medullary inflammation does not reflect the degree of AR (17).

Immunohistochemistry

After fixation in 4% formaldehyde in phosphate-buffered saline and embedding in paraffin, 3- μm -thick slices of kidneys were deparaffinized with Clear Rite (Micom) and rehydrated in descending ethanol series. Sections were then blocked with 10% bovine serum albumin and immunostained using the avidin biotin complex (Vectastain) method with antibodies against human CD3, subunit ϵ - (Abcam), and alkaline phosphatase with antibodies against CD3 ϵ - (Thermo-scientific). After counterstaining with Haemalaun (Merck), images were acquired using an Axio Zeiss microscope (Axiovert 100; Carl Zeiss AG) equipped with a digital camera (AxioCamMRc; Carl Zeiss AG) with the AxionVisonLE Release 4.7.1 software (Carl Zeiss AG). Control stainings included images without primary antibody. The number of CD-positive cells was quantified in 10 fields of views (350 \times 250 μm each) using ImageJ/FRET software (downloadable at <http://rsb.info.nih.gov/ij/>) (18).

Flow Cytometry

T-lymphocyte purity of isolated cells was verified by staining with CD4 $^+$ -APC, CD8 $^+$ -PE, CD3 $^+$ -FITC, and CD45 $^+$ -PerCP-Cy5.5 (BD Biosciences) and subsequent fluorescence-activated cell sorting analysis as described previously (19).

Real-Time (RT) Polymerase Chain Reaction (PCR)

Expression profiles of selected marker genes for infiltrating cells were validated by RT PCR, which was performed using SYBR Green PCR Master Mix or TaqMan Universal PCR Master Mix on an ABI Prism 7700 Sequence Detection System. Table 1 lists the specific

TABLE 1
Sequences of Primers Used for RT PCR

Gene	Primer	
	Sense	Antisense
Glyceraldehyde-3-phosphate dehydrogenase	CATCAACGACCCCTTCATTGAC	ACTCCACGACATACTCAGCACC
CD3d	TTCAAGATAGAAGTGGTT GAATATG	CACCTCCTCGCCAGCTC C
CD8b	GCTTGACATGTGGCCTCATTAC	CGTGGGCGCGGATCATTTGTG

primer pairs that were used. All instruments and reagents were purchased by Applied Biosystems. Relative gene expression values were evaluated with the $2^{-\Delta\Delta C_t}$ method using glyceraldehyde-3-phosphate dehydrogenase as a housekeeping gene.

Statistics

Data were compared by ANOVA with a Scheffé multiple-comparisons test. Data are presented as mean value \pm SEM (n = number of rats, samples, or experiments). Significance was inferred at the P less than 0.05 level.

RESULTS

Flow Cytometry and Labeling of Isolated T lymphocytes

Flow cytometry analysis with CD45 as a general marker for leukocytes and CD3 as a specific marker for T cells revealed a mean T-lymphocyte purity of approximately 90% (n = 3). Supplemental Figure 1 (available online only at <http://jnm.snmjournals.org>) shows a representative experiment in which about 60% of the isolated cells belong to the subpopulation of CD4⁺ T-helper cells and about 30% are part of the group of CD8⁺ cytotoxic T-effector cells (CD4⁺/CD8⁺ ratio, 1:9).

The mean labeling efficiency of T lymphocytes with ¹⁸F-FDG using physiologic saline was 5.4% \pm 2.1%. To elevate ¹⁸F-FDG labeling efficiency by means of stimulating insulin-dependent glucose transporters (GLUT), for example, GLUT4, T cells were coincubated with insulin and K⁺. However, neither the addition

of insulin (6.0% \pm 2.0%) or K⁺ (6.4% \pm 2.6%) nor the combination of insulin and K⁺ (6.6% \pm 3.0%) significantly increased the ¹⁸F-FDG uptake in T lymphocytes (Fig. 1A).

Labeling stability slowly decreased in vitro over time. Retention of the radionuclide in the cells declined from 80.7% \pm 0.64% after 10 min to 71.25% \pm 0.46% after 30 min to 56.42% \pm 1.14% after 60 min, finally reaching 45.2% \pm 0.97% after 120 min (Fig. 1B).

PET Image Analysis and Quantitative Evaluation

In allografts undergoing AR (POD4), we detected a clearly elevated T-lymphocyte signal already at 1 h after injection, which had only slightly increased further after 2 h (Fig. 2A; Supplemental Fig. 2). The quantification of ¹⁸F-FDG-labeled T-cell accumulation as percentage injected dose (%ID) within the parenchyma of the investigated kidneys revealed a significant increase in allografts only (aTX: 1.07 \pm 0.28 %ID after 1 h, n = 7, and 1.18 \pm 0.32 %ID after 2 h, n = 7, P < 0.0001 vs. all other controls), when compared with native control kidneys (0.49 \pm 0.18 %ID, n = 17, and 0.44 \pm 0.15 %ID, n = 16) and sTX (0.55 \pm 0.11 %ID, n = 7, and 0.61 \pm 0.14 %ID, n = 5), CSA toxicity (0.34 \pm 0.07 %ID, n = 10, and 0.39 \pm 0.18 %ID, n = 10), and kidneys with IRI (0.37 \pm 0.14 %ID, n = 6, and 0.40 \pm 0.20 %ID, n = 6) (Fig. 2B).

Autoradiography

Assessment of inflamed tissue by autoradiography confirmed that accumulation of ¹⁸F-FDG-labeled cells correlated to the degree of infiltration. Therefore, we chose autoradiography as a reference method to validate PET results with ¹⁸F-FDG-labeled T lymphocytes. As described previously, POD4 was chosen because accumulation of radiolabeled T cells reached significance at that time, whereas graft integrity was still maintained. On POD4, mainly the renal cortex but also the medulla of aTX kidneys demonstrated a significant accumulation of radiolabeled cells (Supplemental Fig. 3). Allografts exhibited a nearly 4-fold increased tracer uptake, when compared with native control kidneys, isografts, kidneys with IRI, and kidneys with acute CSA toxicity (Table 2).

Histology

To estimate renal damage and infiltration for validation of ¹⁸F-FDG data, we evaluated renal histology and quantified the number of CD3-positive infiltrating T lymphocytes. In allografts, we found distinct signs of acute rejection (marked

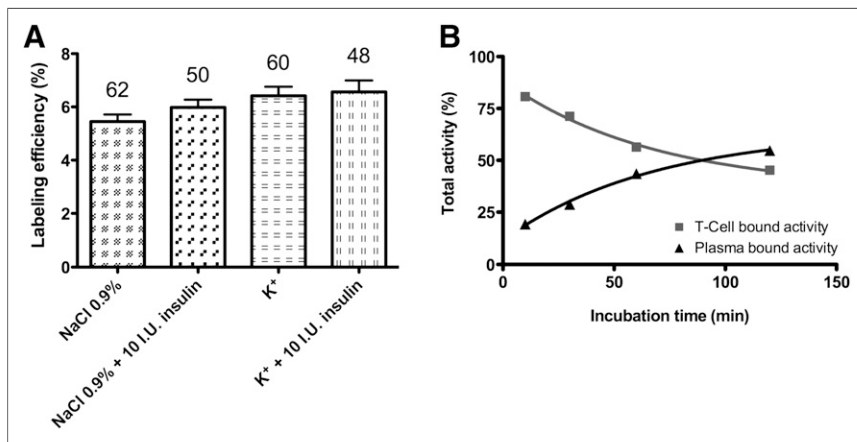


FIGURE 1. (A) T lymphocytes were labeled with ¹⁸F-FDG under different conditions, and labeling efficiency was calculated as ratio between pelleted cells and supernatant. Neither K⁺ or insulin nor the combination of both significantly influenced labeling efficiencies (P > 0.05). Mean value \pm SEM with number of observations indicated above bar (n = 3, 5×10^6 cells, 7 MBq, P > 0.05). (B) Labeling stability was analyzed after 10, 30, 60, and 120 min. Retention of radionuclide in T cells slowly decreased from 80.7% \pm 0.64% after 10 min to 45.2% \pm 0.97% after 120 min (n = 7–8, P < 0.05 for all time points).

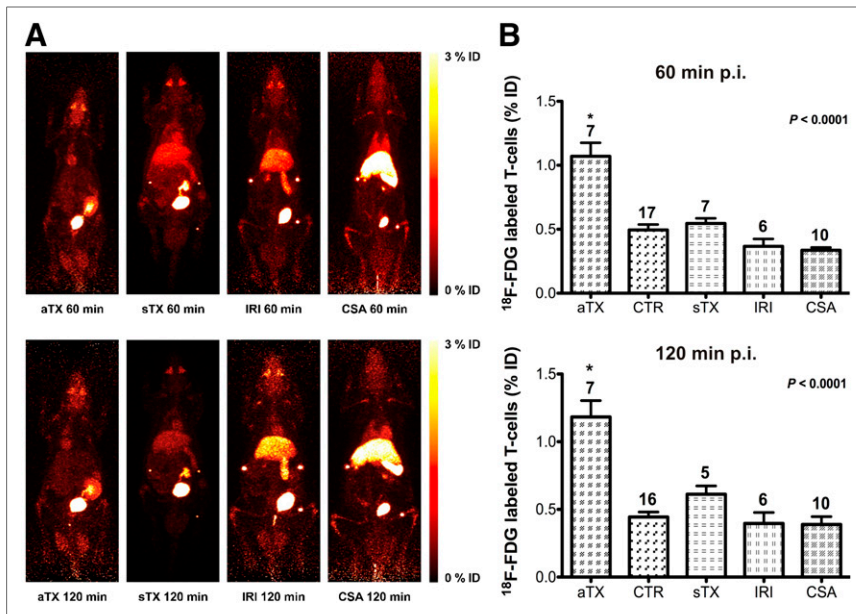


FIGURE 2. (A) Representative PET images (day 4 after surgery) of dynamic whole-body acquisitions of aTX and sTX rats, rats with ATN, and rats with acute CSA toxicity. Effects are summarized after tail vein injection of 30×10^6 ^{18}F -FDG-labeled T cells (maximum-intensity projection, whole-body acquisition for 20 min at 60 min [50–70 min after injection] and at 120 min [110–130 min after injection]). (B) Accumulation of radiolabeled T lymphocytes was calculated as %ID \pm SEM in kidneys with acute rejection (aTX) and controls. On POD4, aTX kidneys exhibited significantly elevated ^{18}F -FDG uptake in comparison to native controls ($P < 0.0001$). Accumulation of labeled cells in kidneys with IRI or acute CSA toxicity and sTX was not significantly different from native controls (all groups $n = 5$ –17). Renal pelvis can contain eliminated free ^{18}F -FDG. Therefore, it was excluded from measurements. Moreover, in sTX, IRI, and CSA toxicity, ^{18}F -FDG-marked pins have been used for orientation reasons during image acquisition. Mean value \pm SEM with number of observations indicated above bars. *Statistical significance to all other groups ($P < 0.05$). CTR = control; p.i. = after injection.

glomerulitis, tubulitis, and endothelialitis) and a highly significant infiltration with CD3-positive T cells in all grafts on POD4 (Fig. 3A; Supplemental Fig. 4). As demonstrated, histologic signs of rejection or significant infiltration were absent in controls (Fig. 3A; Supplemental Fig. 4). However, renal damage according to the induced injury was present, for example, mild tubulitis or detachment of cells into the tubular lumen (ATN) or hyaline arteriolar thickening (CSA toxicity).

To validate our data, transferred T lymphocytes were stained with a human-specific antibody against the CD3 ϵ -subunit. Although all kidneys were perfused for further histologic analysis, at least some CD3-positive cells were found in the cortex of renal allografts undergoing acute rejection (aTX), whereas more or less no human cells could be documented in controls (sTX, CSA toxicity, ATN) (Supplemental Fig. 4).

Correlation of PET Data and Histology

To verify our hypothesis that graft infiltration with radiolabeled T cells is directly related to the degree of inflammation in AR, we correlated the number of CD3-positive cells per field of view of each group to their corresponding %ID. This correlation was found to be significant ($R^2 = 0.61$) (Fig. 3B).

RT PCR Analysis

We used RT PCR analysis ($n = 5$ /group) to confirm and characterize inflammatory cell pattern in aTX. Analysis of the aTX

graft revealed distinct upregulation of CD3 and CD8b on POD4 (Table 3). Upregulation of CD3 and CD8b was absent in iso-grafts (sTX), IRI, and CSA toxicity, confirming the absence of AR or T-cell accumulation. Notably, messenger RNA (mRNA) expression of CD3 and CD8b significantly correlated with the accumulation of ^{18}F -FDG-labeled T cells ($R^2 = 0.41$ and 0.40).

DISCUSSION

Episodes of AR are characterized by a distinct inflammation pattern (20), where leukocytes, mainly activated T lymphocytes, are recruited into the transplant (21). The updated Banff classification categorizes infiltration and finally scores renal transplant rejection (1,22,23). At present, core needle biopsy is the gold standard in the definite diagnosis of AR. However, as an invasive method it bears the risk of severe graft injury. Moreover, it is not feasible in patients receiving anticoagulation therapy and might present false-negative results, if AR is focal or patchy (6).

Because activated leukocytes highly accumulate ^{18}F -FDG, which can be assessed by PET, we recently established ^{18}F -FDG PET for the noninvasive detection and monitoring of renal allograft rejection (9). Moreover, ^{18}F -FDG PET can be applied for the early evaluation of immunosuppressive treatment response and

might assist in the differential diagnosis of AR, ATN, and acute CSA toxicity (8).

Nevertheless, potential drawbacks of ^{18}F -FDG are, on the one hand, urinary excretion of ^{18}F -FDG and drainage into the renal pelvis, aggravating assessment of parenchymal glucose metabolism, potentially inducing false-positive ^{18}F -FDG signaling, and requiring late acquisitions to reduce urinary ^{18}F -FDG. On the other hand, ^{18}F -FDG uptake represents unspecific metabolic activity. Thus, especially graft infection or potentially also lymphoma might generate a similar ^{18}F -FDG accumulation pattern (24). Although clinical symptoms and additional serologic and image-based methods can assist in the differential diagnosis, a more specific tracer would be desirable. Because recruitment of T lymphocytes does not play a leading role in the development of infection, this diagnosis most likely can be ruled out using PET with radiolabeled T cells. Moreover, using ^{18}F -FDG PET for the detection of AR, we applied PET assessment 3 h after injection for several reasons, such as ^{18}F -FDG drainage or elimination of free ^{18}F -FDG. Although this is earlier than diagnostics by histologic evaluation in most cases, an easy and fast translation into the clinics might be challenging.

In this study, we present PET with ex vivo ^{18}F -FDG-labeled human T lymphocytes as a highly specific diagnostic tool to assess AR occurring in an allogeneic rat renal transplantation model. Infiltration of radiolabeled T lymphocytes in all used renal injury

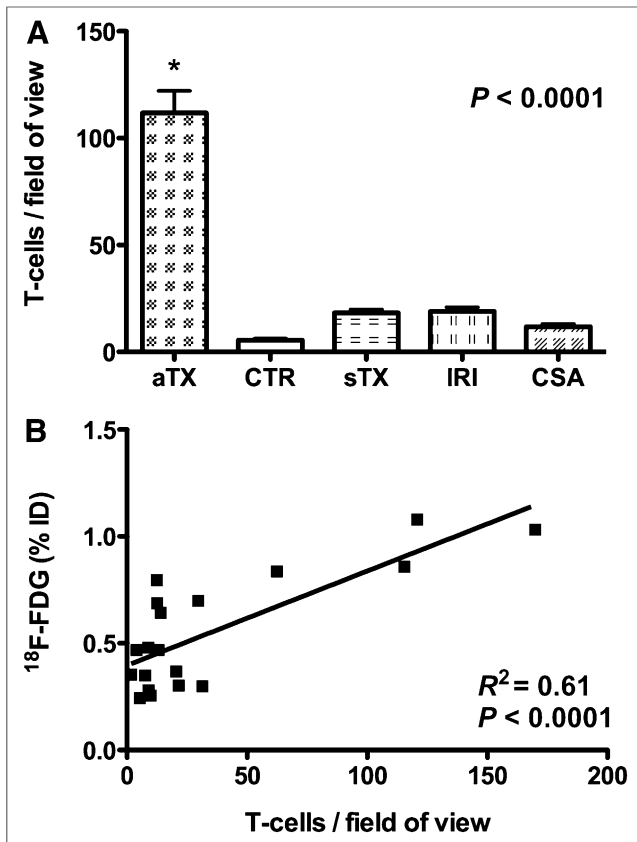


FIGURE 3. (A) Semiautomated quantification of infiltration by CD3-positive T cells (as evaluated by light microscopy) exhibits significant inflammation pattern in renal allografts when compared with all other controls. Mean value \pm SEM with number of observations indicated above bars. *Statistical significance to all other groups ($P < 0.05$). (B) Correlation of accumulation of radiolabeled T cells as %ID and of infiltrating CD3-positive T cells in different groups of kidneys. Significant correlation of ^{18}F -FDG signal and infiltrating leukocytes and T cells was found ($R^2 = 0.61$). CTR = control.

and transplant models was quantitatively evaluated from PET images and calculated as %ID. Allografts developing AR exhibit a significant elevation of %ID on POD4, when compared with isografts. POD4 was chosen because signs of AR clearly occur on POD4 (9), whereas graft perfusion and function are still preserved. Consistently, injured kidneys with common differential diagnoses of AR, namely ATN and acute CSA toxicity, did not show any accumulation of radiolabeled T cells. Using ^{18}F -FDG-labeled leukocytes, Toso et al. tried to assess AR of pancreatic

TABLE 2
Accumulation of ^{18}F -FDG-Labeled T Lymphocytes (Autoradiographic Analysis)

Kidney part	aTX	sTX	IRI	CSA toxicity
Cortex	3.98*	1.38	1.12	0.91
Medulla	3.76*	1.53	1.26	0.85

* $P < 0.001$.
Accumulation of radiolabeled T cells in renal medulla and cortex was assessed by autoradiography, expressed as radioactivity ratio of respective tissue sample and native controls. $n = 5/\text{group}$.

islet transplants in the liver. Their approach remained unsuccessful because of the well-known free ^{18}F -FDG uptake in the liver (background activity) (25).

To elevate ^{18}F -FDG-labeling efficiency, T cells were coincubated with insulin and K^+ . However, neither the addition of insulin or K^+ nor the combination of insulin and K^+ significantly increased the ^{18}F -FDG uptake in T cells (Fig. 1). These results are concordant with those in the literature because T lymphocytes mainly express the insulin-independent GLUT1 and GLUT3 (26) and do not respond to insulin with an upregulation of GLUTs (27). Interestingly, Botti et al. were able to demonstrate much higher labeling efficiencies. However, they used lower amounts of radioactivity for cell incubation, resulting in a better ratio of radioactivity to cell number in their experiments (28).

To validate our PET data, we correlated the entirely imaged-based measurements of T-cell accumulation to results from reference methods, for example, histologic quantification of infiltration (leukocytes, CD3-positive T lymphocytes) (Fig. 3; Supplemental Fig. 4) and mRNA expression of T-cell markers within the kidneys (Table 3). We found a significant correlation between enhanced accumulation of radiolabeled T cells and histologic infiltration (Fig. 3). In contrast, native controls showed a low ^{18}F -FDG uptake only, which also correlated with the histologic findings. In addition, sTX, as well as kidneys with ATN and acute CSA toxicity, exhibited only marginal histologic signs of infiltration, again correlating well with the ^{18}F -FDG uptake. These results were supported by RT PCR analysis of marker genes. As commonly observed during AR (10), we detected significant mRNA upregulations of activated T-lymphocyte surface antigens such as CD3 and CD8b in renal allografts on POD4. These upregulations were absent in sTX, ATN, and CSA toxicity (Table 3). Notably, the expression of CD3 and CD8b significantly correlated with accumulation of ^{18}F -FDG-labeled T lymphocytes in all measured groups.

TABLE 3
RT PCR-Based Characterization of T-Lymphocyte Infiltration in Different Groups of Kidneys on Day 4 After Surgery

Cell type	mRNA	aTX	sTX	IRI	CSA toxicity
T cells	CD3	100.6 \pm 12.7*	2.4 \pm 0.3	3.2 \pm 0.3	1.5 \pm 0.2
Cytotoxic T cells	CD8b	115.8 \pm 12.6*	1.4 \pm 0.2	2.3 \pm 0.2	1.6 \pm 0.5

*Significantly increased relative to control ($P < 0.0001$).
Data are mean values (compared with control values, $n = 4-6$) \pm SEM.

As a third reference method, autoradiography revealed a significantly higher accumulation of radiolabeled cells in allogeneic transplants than in native controls and kidneys with ATN, acute CSA toxicity, or sTX (Table 2). In detail, allografts exhibited a nearly 4-fold increased activity when compared with control kidneys (native controls, sTX, IRI, and CSA toxicity). Taken together, these results indicate that PET with radiolabeled T cells is not only able to diagnose, but also able to quantify AR and thereby represent its histologic degree of inflammation.

The use of radiolabeled cells has several advantages in comparison to conventional ^{18}F -FDG PET imaging. First, despite the low amount of radioactivity contained within the radiolabeled T cells, a strong signal can be detected in renal allografts, militating in favor of a potential higher sensitivity, while simultaneously reducing the patient's radiation dose to a minimum.

Second, less urinary excretion of free ^{18}F -FDG was documented, which potentially could lead to false-positive results. In humans, PET imaging using ^{18}F -FDG-labeled leukocytes leads to less than 10% leakage of free ^{18}F -FDG in the urinary system after 6 h (29). Our *in vitro* labeling stability studies revealed that the amount of free ^{18}F -FDG slowly increases over time (Fig. 1B). This increase has also been shown by Botti et al. who assessed the liberation rate of ^{18}F -FDG in T cells (28). However, because urine microscopy after PET scans did not reveal relevant amounts of T cells (data not shown), the activity shown in the bladder accounts at least in part to free ^{18}F -FDG.

Most likely, the activity was released by (destroyed) T cells. In cases of acute rejection, some of this ^{18}F -FDG should be delivered by T cells to the kidney and locally released. However, we assessed the bladder activity in all groups of rats and could not find differences between the groups (~ 2 – 3 %ID). Thus, liberation of activity was equal in all groups, leading us to the conclusion that activity is probably released from destroyed cells, which have been affected, for example, by the immune response. This finding is supported by data from Pellegrino et al. who analyzed the form of ^{18}F -FDG trapped in ^{18}F -FDG-labeled white blood cells (30). They observed that the chemical form of ^{18}F as analyzed by thin-layer radiochromatography demonstrated that virtually all radioactivity inside the white blood cells was present as ^{18}F -FDG-6P, a chemical form incapable of egression from the cell and minimally reconverted to ^{18}F -FDG.

Third, using radiolabeled lymphocytes, PET can be applied as early as 1 h after injection, thereby significantly accelerating the diagnostic procedure. The T-cell ^{18}F -FDG signal of aTX subsequently increased after injection of T cells, reaching a significant difference, compared with the native kidney, at 30–50 min after the injection. The time point 50–70 min was chosen because it combined a significant increase in ^{18}F -FDG signal with a good visual delineation of the graft.

One might question the fact that xenogene cells were used for the detection of AR. However, this has been established before. Wang et al. performed *in vivo* PET imaging using human cells in a Parkinson disease rat model (31), and Hay et al. used human ^{111}In -labeled leukocytes to assess inflammatory lesions in rats (32). Moreover, imaging of total-body T-cell distribution in our rats exhibited a distinct allocation, with a primary emphasis on the reticuloendothelial system and was comparable to the biodistribution of ^{18}F -FDG-labeled leukocytes in healthy humans.

Imaging using *ex vivo* radiolabeled leukocytes is a well-established method that found its way into daily clinical routine particularly in the diagnosis of inflammatory and infectious

disorders (e.g., scintigraphy using ^{111}In - and $^{99\text{m}}\text{Tc}$ -labeled leukocytes) (33–36). Because recruitment and activation of inflammatory cells, especially T lymphocytes, play a pivotal role in AR, there have been efforts made to image graft infiltration by means of radiolabeled cells. SPECT-based imaging with ^{111}In - and $^{99\text{m}}\text{Tc}$ -labeled leukocytes has already been used to assess AR in a small cohort of intestinal and kidney transplant recipients (37,38). However, PET has the advantage of a quantitative analysis (assessment of %ID or standardized uptake value), which is useful in the diagnosis of allograft rejection and for monitoring patients' responses to therapy. Thus, PET with ^{18}F -FDG-labeled autologous T lymphocytes might be translated to humans in the near future.

CONCLUSION

We present and validate an entirely imaging-based noninvasive method to assess AR using PET with ^{18}F -FDG-labeled T lymphocytes. Requiring extremely low radioactive doses, this method is highly specific and can differentiate between AR and ATN. A clinical translation to investigate the kinetics of AR and the response to therapeutic intervention seems promising.

DISCLOSURE

The costs of publication of this article were defrayed in part by the payment of page charges. Therefore, and solely to indicate this fact, this article is hereby marked "advertisement" in accordance with 18 USC section 1734. This study was supported in part by the Interdisciplinary Centre for Clinical Research Münster, Germany (IZKF, Core Unit PIX), and the Deutsche Forschungsgemeinschaft (SFB 656 C7 and C6). No other potential conflict of interest relevant to this article was reported.

ACKNOWLEDGMENTS

We are grateful to Anne Kanzog, Christine Bätza, Ute Neugebauer, Rita Schröter, Wiebke Gottschlich, Sandra Schröer, Irmgard Hoppe, and Roman Priebe for excellent technical assistance and to Daniel Burkert and Sven Fatum for producing radiotracers.

REFERENCES

1. Racusen LC, Solez K, Colvin RB, et al. The Banff 97 working classification of renal allograft pathology. *Kidney Int.* 1999;55:713–723.
2. Rush D. Protocol transplant biopsies: an underutilized tool in kidney transplantation. *Clin J Am Soc Nephrol.* 2006;1:138–143.
3. Morath C, Ritz E, Zeier M. Protocol biopsy: what is the rationale and what is the evidence? *Nephrol Dial Transplant.* 2003;18:644–647.
4. El-Mekresh M, Osman Y, Ali-El-Dein B, El-Diasty T, Ghoneim MA. Urological complications after living-donor renal transplantation. *BJU Int.* 2001;87:295–306.
5. Schwarz A, Hiss M, Gwinner W, Becker T, Haller H, Keberle M. Course and relevance of arteriovenous fistulas after renal transplant biopsies. *Am J Transplant.* 2008;8:826–831.
6. Solez K, Axelsen RA, Benediktsson H, et al. International standardization of criteria for the histologic diagnosis of renal allograft rejection: the Banff working classification of kidney transplant pathology. *Kidney Int.* 1993;44:411–422.
7. Grabner A, Schnöckel U, Kentrup D, Schäfers M, Reuter S. Strategies for non-invasive molecular imaging of acute allograft rejection by gamma scintigraphy and positron emission tomography. *Curr Radiopharm.* 2011;4:10–23.
8. Reuter S, Schnöckel U, Edemir B, et al. Potential of noninvasive serial assessment of acute renal allograft rejection by ^{18}F -FDG PET to monitor treatment efficiency. *J Nucl Med.* 2010;51:1644–1652.
9. Reuter S, Schnöckel U, Schröter R, et al. Non-invasive imaging of acute renal allograft rejection in rats using small animal F-FDG-PET. *PLoS ONE.* 2009;4:e5296.

10. Nিকেলেইট V, Andreoni K. Inflammatory cells in renal allografts. *Front Biosci.* 2008;13:6202–6213.
11. Cornell LD, Smith RN, Colvin RB. Kidney transplantation: mechanisms of rejection and acceptance. *Annu Rev Pathol.* 2008;3:189–220.
12. Ingulli E. Mechanism of cellular rejection in transplantation. *Pediatr Nephrol.* 2010;25:61–74.
13. Velic A, Gabriels G, Hirsch JR, et al. Acute rejection after rat renal transplantation leads to downregulation of NA⁺ and water channels in the collecting duct. *Am J Transplant.* 2005;5:1276–1285.
14. Velic A, Hirsch JR, Bartel J, et al. Renal transplantation modulates expression and function of receptors and transporters of rat proximal tubules. *J Am Soc Nephrol.* 2004;15:967–977.
15. Schnöckel U, Reuter S, Stegger L, et al. Dynamic ¹⁸F-fluoride small animal PET to noninvasively assess renal function in rats. *Eur J Nucl Med Mol Imaging.* 2008;35:2267–2274.
16. Schäfers KP, Reader AJ, Kriens M, Knoess C, Schober O, Schäfers M. Performance evaluation of the 32-module quadHIDAC small-animal PET scanner. *J Nucl Med.* 2005;46:996–1004.
17. Sis B, Sarioglu S, Celik A, et al. Renal medullary changes in renal allograft recipients with raised serum creatinine. *J Clin Pathol.* 2006;59:377–381.
18. Feige JN, Sage D, Wahli W, Desvergne B, Gelman L. PixFRET, an ImageJ plugin for FRET calculation that can accommodate variations in spectral bleed-throughs. *Microsc Res Tech.* 2005;68:51–58.
19. Di Marco GS, Reuter S, Hillebrand U, et al. The soluble VEGF receptor sFlt1 contributes to endothelial dysfunction in CKD. *J Am Soc Nephrol.* 2009;20:2235–2245.
20. Sarwal M, Chua MS, Kambham N, et al. Molecular heterogeneity in acute renal allograft rejection identified by DNA microarray profiling. *N Engl J Med.* 2003;349:125–138.
21. Edemir B, Reuter S, Borgulya R, et al. Acute rejection modulates gene expression in the collecting duct. *J Am Soc Nephrol.* 2008;19:538–546.
22. Solez K, Colvin RB, Racusen LC, et al. Banff 07 classification of renal allograft pathology: updates and future directions. *Am J Transplant.* 2008;8:753–760.
23. Sis B, Mengel M, Haas M, et al. Banff'09 meeting report: antibody mediated graft deterioration and implementation of Banff working groups. *Am J Transplant.* 2010;10:464–471.
24. Reuter S, Rahbar K, Busch V, et al. Acute renal failure due to primary bilateral renal large B-cell lymphoma: diagnostics and follow-up by FDG-PET/CT. *Clin Nucl Med.* 2009;34:722–724.
25. Toso C, Zaidi H, Morel P, et al. Assessment of ¹⁸F-FDG-leukocyte imaging to monitor rejection after pancreatic islet transplantation. *Transplant Proc.* 2006;38:3033–3034.
26. Fu Y, Maianu L, Melbert BR, Garvey WT. Facilitative glucose transporter gene expression in human lymphocytes, monocytes, and macrophages: a role for GLUT isoforms 1, 3, and 5 in the immune response and foam cell formation. *Blood Cells Mol Dis.* 2004;32:182–190.
27. Maratou E, Dimitriadis G, Kollias A, et al. Glucose transporter expression on the plasma membrane of resting and activated white blood cells. *Eur J Clin Invest.* 2007;37:282–290.
28. Botti C, Negri DR, Seregni E, et al. Comparison of three different methods for radiolabelling human activated T lymphocytes. *Eur J Nucl Med.* 1997;24:497–504.
29. Forstrom LA, Dunn WL, Mullan BP, Hung JC, Lowe VJ, Thorson LM. Biodistribution and dosimetry of [¹⁸F]fluorodeoxyglucose labelled leukocytes in normal human subjects. *Nucl Med Commun.* 2002;23:721–725.
30. Pellegrino D, Bonab AA, Dragotakes SC, Pitman JT, Mariani G, Carter EA. Inflammation and infection: imaging properties of ¹⁸F-FDG-labeled white blood cells versus ¹⁸F-FDG. *J Nucl Med.* 2005;46:1522–1530.
31. Wang R, Zhang J, Guo Z, et al. In-vivo PET imaging of implanted human retinal pigment epithelium cells in a Parkinson's disease rat model. *Nucl Med Commun.* 2008;29:455–461.
32. Hay RV, Skinner RS, Newman OC, et al. Scintigraphy of acute inflammatory lesions in rats with radiolabelled recombinant human interleukin-8. *Nucl Med Commun.* 1997;18:367–378.
33. Dumarey N, Egrise D, Blocklet D, et al. Imaging infection with ¹⁸F-FDG-labeled leukocyte PET/CT: initial experience in 21 patients. *J Nucl Med.* 2006;47:625–632.
34. Dumarey N. Imaging with FDG labeled leukocytes: is it clinically useful? *Q J Nucl Med Mol Imaging.* 2009;53:89–94.
35. Peters AM, Danpure HJ, Osman S, et al. Clinical experience with ^{99m}Tc-hexamethylpropylene-amineoxime for labelling leucocytes and imaging inflammation. *Lancet.* 1986;2:946–949.
36. Papós M, Nagy F, Lang J, Csernay L. Leukocyte scintigraphy to assess disease activity in inflammatory bowel disease [letter]. *J Nucl Med.* 1996;37:400.
37. Watson CJ, Wraight EP, Neale G, Jamieson NV, Friend PJ, Calne R. Radionuclide studies in intestinal transplantation: diagnosis of rejection and assessment of permeability. *Transplantation.* 1996;61:155–157.
38. Lopes de Souza SA, Barbosa da Fonseca LM, Torres GR, et al. Diagnosis of renal allograft rejection and acute tubular necrosis by ^{99m}Tc-mono-nuclear leukocyte imaging. *Transplant Proc.* 2004;36:2997–3001.